

## ANALYTICAL MODELING OF DUAL ACTUATED COMPLIANT BEAM MICROGRIPPER SYSTEM

NAYYER ABBAS ZAIDI

*Faculty of Electronic Engineering, Ghulam Ishaq Khan Institute of Engineering Sciences and Technology, Pakistan  
e-mail: nayyer@giki.edu.pk*

SHAFAT A. BAZAZ

*Department of Computer Science, Centre for Advance Studies in Engineering (CASE), Islamabad, Pakistan  
e-mail: bazaz@case.edu.pk*

This paper presents the analytical modeling for the design of a microgripper system that comprises dual jaw actuation mechanism with real-time contact sensing. The interdigitated lateral comb-drive based electrostatic actuator is used to move the gripper arms. Simultaneous contact sensing is achieved through a transverse comb based capacitive sensor, to detect the contact between the jaws and microobject. The detailed analytical modeling of the microgripper reveals that the stresses induced in the structure is well below the maximum yield stress of 7000 MPa for single crystal silicon. The fabricated microgripper produced a displacement of 16  $\mu\text{m}$  at gripper jaws for the applied actuation voltage of 45 V, which is approximately the same as predicted by the analytical model.

*Keywords:* compliant structure, contact sensing, linear amplification, microgripper, micro-manipulation

### 1. Introduction

Expansion in micro and nanotechnologies has raised the need for the development of the micro-tools to handle small scale objects. MEMS based microgrippers are the major focus for many applications like microassembly, micromanuplation and microsurgery. Microgrippers based on the electrostatic actuation are ideal because of low power consumption, satisfactory amount of force, no hysteresis and ease in fabrication. Microgrippers based on the electrostatic actuation were presented in Volland *et al.* (2002), Beyeler *et al.* (2007). Both of these designs operate on high DC voltages. Moreover, in these designs only one gripper jaw is actuated while other is connected to the capacitive force sensor. The first jaw keeps dragging and pushing the object during its motion till it touches the second jaw and transfers the force to it. This single jaw movement operation increases the probability of damaging the micro-object.

In this paper, an electrostatically actuated microgripper design, fabricated using standard micromachining process SOI-MUMPs is developed (Miller *et al.*, 2004). This microgripper operates at 0 to 45 V actuation voltages. The lateral comb-drive actuation mechanism is used to produce movement in both jaws to enhance the gripping force. The microgripper is integrated with the transverse comb-drive which acts as a contact sensor. The purpose of this contact sensor is to avoid producing an excessive force at the jaws. This makes it possible to grasp microobjects like biological cells automatically using a closed loop control which makes the whole micromanipulation process easy and time efficient.

The rest of the paper is organized as follows: Section 2 explains the complete operation of the proposed microgripper design. The analytical modeling of microgripper parts which include the cantilever beam design with concentrated end loading, quad-clamped beam design with central distributed mass and gripper arm design are described in Section 3. The actuator and sensor

design is presented in Section 4. Experimental characterization of the microgripper is carried out in Section 5. Finally Section 6, provides the conclusion of our work.

## 2. Theory of operation

The proposed microgripper, as shown in Fig. 1, consists of three parts: a) actuator, b) sensor and c) gripper jaws. The design uses dual electrostatic actuation system, i.e. there are two separate electrostatic actuators for the simultaneous movement of two jaws. Each actuator consists of a set of stator combs interdigitated with a set of rotor combs. DC voltages applied to both the actuators simultaneously, which moves the central beam in upward direction. This movement of central beam is amplified at the gripper jaws due to the integrated action of the gripper arm and the vertical beam. A transverse comb-drive based capacitive contact sensor is included along each of the two central beams in between the gripper arm and actuator as shown in Fig. 1. The change in the gap between the overlap length of the sensor combs results in the change in capacitance. This change in capacitance is measured through universal capacitance readout chip MS3110 that produces voltage proportional to the change in capacitance (Universal Capacitive readout, 2004). When the object is gripped between the gripper jaws, then no capacitance change is detected by the universal capacitance readout chip. This indicates that the object has been grasped and thus, to avoid any damage to the object, no further actuation voltage is applied.

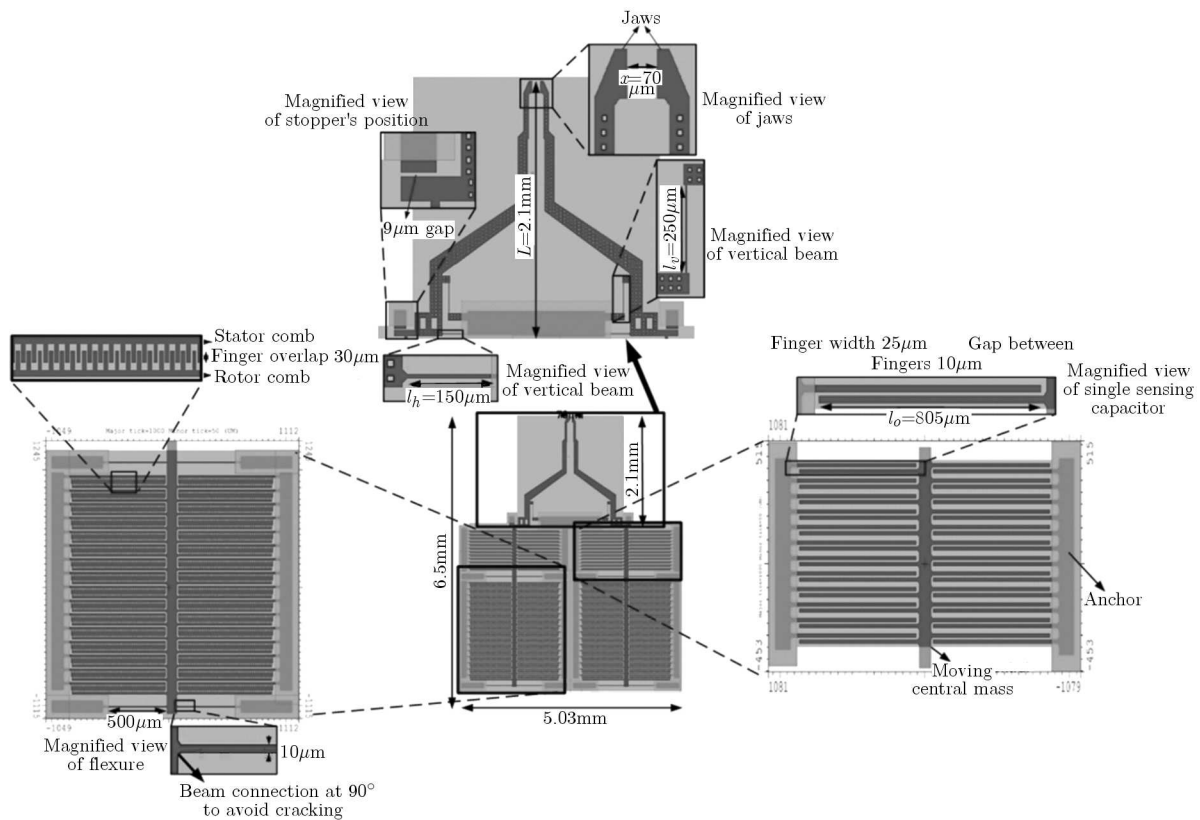


Fig. 1. Complete microgripper design with the integrated capacitive contact sensor

## 3. Microgripper design

The microgripper beam system is primarily composed of: a) cantilever beams with concentrated end loading, b) quad-clamped beams with central distributed mass, c) gripper arm.

### 3.1. Cantilever beam design

The single layer cantilever beam with concentrated end loading is shown in Fig. 2a. Assuming that  $F$  is the loading force caused by the mass  $M$  attached to the free end of the beam, the resulting equation for the bending moment of the cantilever beam is (Bao, 2005)

$$M_{(x)} = -F(L - x) \quad (3.1)$$

The differential equation for the bending moment as a function of moment of inertia  $I$  and displacement function  $w_{(x)}$  is expressed as (Bao, 2005)

$$M_{(x)} = -EIw''_{(x)} \quad (3.2)$$

After solving the above equation and applying boundary conditions  $w_{(0)} = 0$ ,  $w'_{(0)} = 0$  and  $w''_{(L)} = 0$ , we get displacement function as

$$w_{(x)} = \frac{2F(3L - x)x^2}{Ebh^3} \quad (3.3)$$

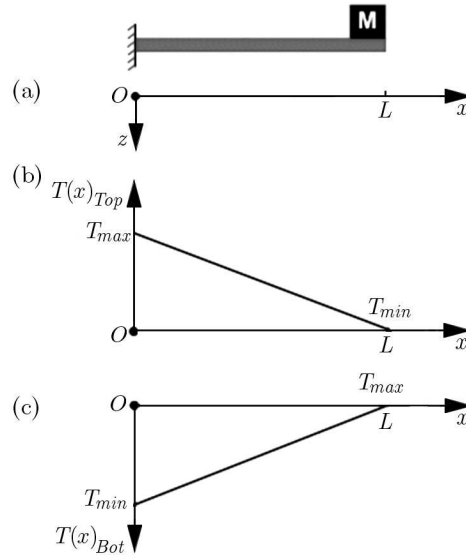


Fig. 2. (a) Single layer cantilever beam with concentrated end loading, (b) stress in the guided cantilever beam at the top surface, (c) stress in the guided cantilever beam at the bottom surface

The maximum displacement will occur at the free end of the cantilever beam i.e., at  $x = L$  and is given as

$$w_{max} = \frac{4FL^3}{Ebh^3} \quad (3.4)$$

Using Hook's law, the restoring force produced by the beam is given as

$$F = kw_{max} \quad (3.5)$$

The spring constant from the above equation is

$$k = \frac{Ebh^3}{4L^3} \quad (3.6)$$

where width, thickness and length of the beam are  $b$ ,  $h$  and  $L$ , respectively. The stresses produced in the cantilever beam at the top and bottom surface with ( $I = bh^3/12$ ) are given as (Bao, 2005)

$$T(x)\Big|_{Top} = \frac{6F}{bh^2}(L-x) \quad T(x)\Big|_{Bottom} = \frac{-6F}{bh^2}(L-x) \quad (3.7)$$

Figures 2b and 2c show stress variations at the top and bottom surface with respect to the distance  $x$  from the fixed end of the beam as the force  $F$  is applied at the free end. The stress has its maximum value at the insertion point of the top of the cantilever beam with the support and it decreases linearly to zero at the end where the mass is attached.

The maximum values of stress calculated for the top surface of the horizontal and vertical beams are 424.8 MPa and 708 MPa, respectively. Since the bottom surface of the beam is compressed during bending, so the maximum stress at the bottom surface for both the horizontal and vertical beam is zero and the minimum stress is  $-424$  MPa for horizontal beam and  $-708$  MPa for the vertical beam. These stress values, calculated for both the top and bottom surfaces of the beam, are much less than the yield strength of the single crystal silicon which is 7000 MPa (Petersen, 1982).

### 3.2. Quad-clamped beam design

The microgripper system is suspended on the quad-clamped beam with a central mass. A schematic diagram of the structure is shown in Fig. 3. Due to the symmetry of the beam system,

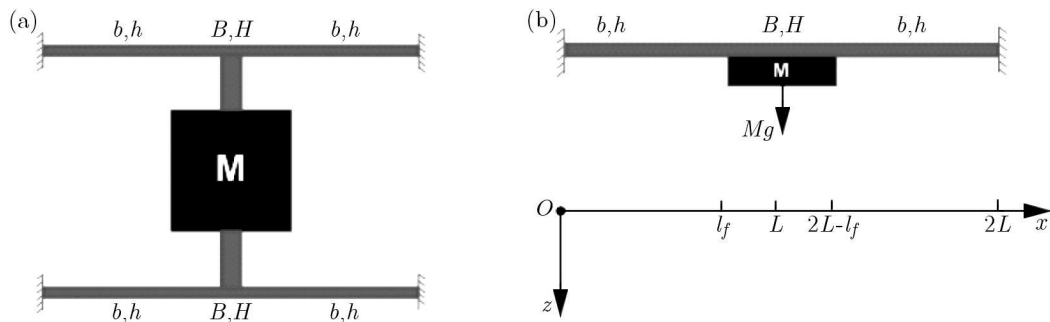


Fig. 3. Single layer quad-clamped beam with central load (a) top view, (b) side view

only one fourth of the structure is to be considered. The bending moment for the bottom left beam is expressed as (Bao, 2005)

$$M(x) = F_o x - m_o - \int_0^x \frac{M_b g}{L} (x-s) ds \quad (3.8)$$

where  $F_o$  is the supporting force at the four ends of the quad-clamped beam,  $m_o$  is the reaction moment at the clamped end of the beam to balance the bending moment caused by the loading force  $F$ . The differential equation for bending moment as a function of moment of inertia  $I$  and displacement function  $w(x)$  is expressed as (Bao, 2005)

$$M(x) = -EIw''(x) \quad (3.9)$$

The displacement of the beam can be calculated by applying the boundary conditions  $w(0) = 0$ ,  $w'(0) = 0$ ,  $w'(l_f) = 0$ ,  $w''(l_f/2) = 0$  and assuming that the central mass is much wider and thicker than the beams (the bending of the mass can be negligible) the expression for this displacement is

$$w(x) = \frac{F(3x^2 l_f - 2x^3)}{48EI} \quad (3.10)$$

It will be maximum at  $x = l_f$ , therefore

$$w_{max} = \frac{Fl_f^3}{48EI} \quad (3.11)$$

Using Hook's law, the beam stiffness is derived as

$$F = kw_{max} \quad (3.12)$$

The spring constant is given as

$$k_f = \frac{4Ebh^3}{l_f^3} \quad (3.13)$$

The stresses due to expansion of the top surface and compression of the bottom surface of the beam and with  $I = bh^3/12$  are derived as

$$T(x)|_{Top} = \frac{3F}{4bh^2}(l_f - 2x) \quad T(x)|_{Bottom} = \frac{-3F}{4bh^2}(l_f - 2x) \quad (3.14)$$

The distribution of the stress along the length of the beam is shown in Fig. 4. The stresses on the beam surface vary linearly from a positive maximum at one end to the negative maximum at the other end. The maximum and minimum stresses calculated for the top and bottom surfaces of the quad-clamped beam are 39.85 MPa and -39.85 MPa, respectively. These stress values are less than the yield strength of the single crystal silicon which is 7000 MPa (Petersen, 1982). This ensures that the beam will not undergo permanent deformation for the maximum applied force and will remain in the elastic range. The stress is zero at the midpoint  $x = l_f/2$  of the beam both at the top and at the bottom surfaces.

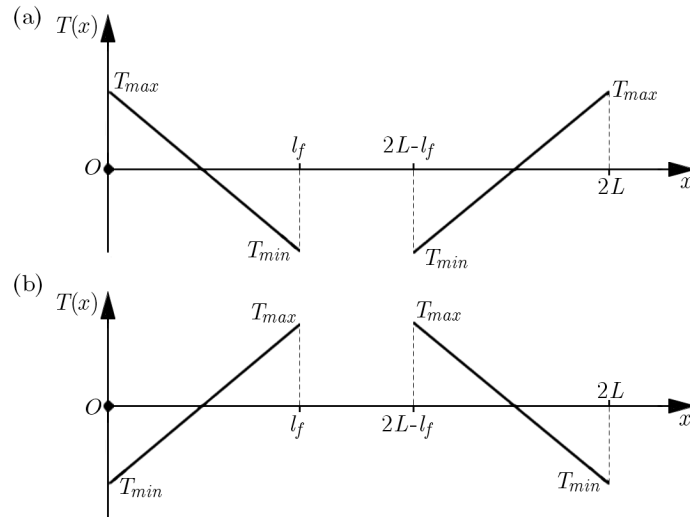


Fig. 4. Stress plot of two beams at one side of the single layer quad-clamped beam on (a) top surface, (b) bottom surface

### 3.3. Gripper arm design

A new gripper arm and jaw with the compliant structure as shown in Fig. 5 has been designed for grasping micro sized objects. The design includes a horizontal and vertical beam to produce the elastic restoring force in the horizontal and vertical direction simultaneously. The vertical beam additionally provides support against the out of plane movement of the gripper arms. The

structure is designed in such a way that it will maintain an angle of  $90^\circ$  between the gripper arm and the horizontal beam. The inner face of the jaw makes the angle  $\psi$  with the  $y$ -axis so that both jaws join parallel to each other upon the application of the force as shown in Fig. 6. Additionally, the jaw moves a small distance along the  $y$ -axis during grasping due to the direction of the applied force. This action ensures that the object completely comes between the jaws while grasping. Two stoppers have been placed near the point of application of the force in order to stop any extra movement of the central beam after the object has been fully grasped. In this design, the vertical displacement produced in the central beam is amplified by a constant factor. When a force is applied by central beam at point  $Q$  of the gripper arm, a moment is produced which makes the rigid mass of the gripper arm to rotate about the point  $O$ . The horizontal and vertical beams act as the moment arms.

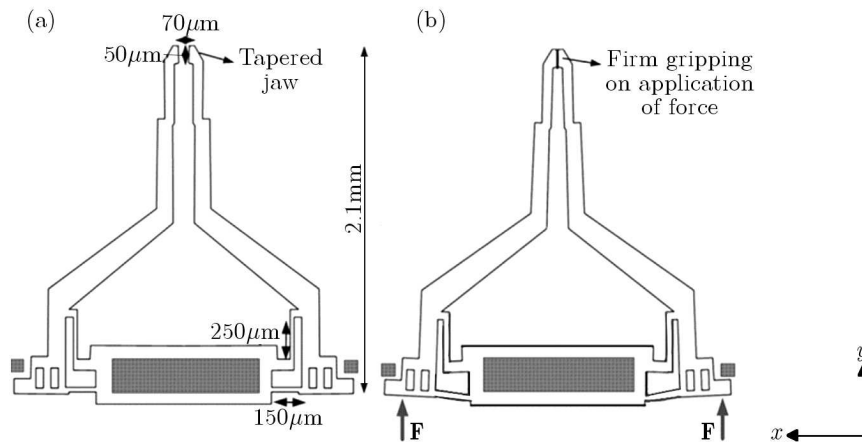


Fig. 5. Gripper arm and beam system design (a) with no force (b) under applied force

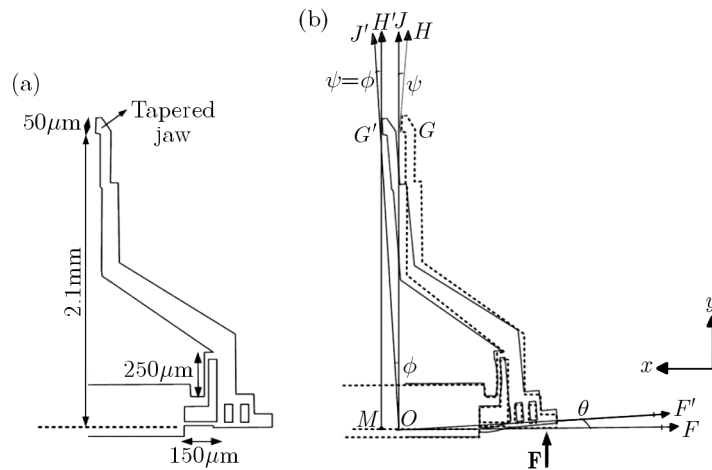


Fig. 6. (a) Right section of the gripper, (b) gripper arm moving mechanism

In order to join both jaws completely and firmly on the point of application of the force at  $F$ , the jaw angle  $\psi$  is designed to be equal to the angle  $\theta$  subtended at  $O$  when the force is applied at the point  $Q$ . Hence

$$\psi = \phi = \theta \tag{3.15}$$

#### 4. Gripper actuator and sensor design

The electrostatic force required for the actuation is given as

$$F = \frac{Nn}{2} \varepsilon \frac{tV^2}{d} \quad (4.1)$$

where  $nN$  is the total number of comb-drives connected in parallel,  $t$  is the thickness,  $d$  is the gap between the comb-drives and  $V$  is the applied voltage.

The horizontal and the quad-clamped beams are connected in parallel, and it is assumed that the force and displacement produced at the free end of the horizontal beam is approximately equal to the force and the displacement produced at the free end of the vertical beam. Thus the spring constant of the overall system is given as

$$K = Et^3 \left( \frac{4b_f}{l_f^3} + \frac{b_h}{4l_h^3} + \frac{b_v}{4l_v^3} \right) \quad (4.2)$$

where  $b_f$  is width of flexure connected to vertical beam,  $l_f$  is length of that flexure,  $b_h$  is width of the horizontal flexure and  $b_v$  is width of the vertical flexure.

Using Hook's law, the resultant force on the vertical beam is given as

$$F = Et^3 \left( \frac{4b_f}{l_f^3} + \frac{b_h}{4l_h^3} + \frac{b_v}{4l_v^3} \right) y \quad (4.3)$$

where  $y$  is the displacement of the central beam along the  $y$ -axis, and from Eq. (4.3) displacement expression is derived as

$$y = \frac{\frac{Nn}{2} \varepsilon \frac{tV^2}{d}}{Et^3 \left( \frac{4b_f}{l_f^3} + \frac{b_h}{4l_h^3} + \frac{b_v}{4l_v^3} \right)} \quad (4.4)$$

Considering the fact that tangents of  $\psi$ ,  $\phi$  and  $\theta$  in Fig. 6b are equal, the displacement of the gripper jaws in the  $x$ -axis is derived as

$$X = \frac{L}{l_Q} \frac{\frac{Nn}{2} \varepsilon \frac{tV^2}{d}}{Et^3 \left( \frac{4b_f}{l_f^3} + \frac{b_h}{4l_h^3} + \frac{b_v}{4l_v^3} \right)} \quad (4.5)$$

where  $L/l_Q$  is the amplification factor of the displacement at the tip of the gripper jaws, where  $L = 2.1$  mm is the length of the microgripper jaws and  $l_Q = 150$   $\mu$ m is the length of the horizontal flexure as shown in Fig. 6a.

In the transverse comb-drive based differential sensor, the capacitance on one side of the comb-drive increases and decreases by same proportion on the opposite side of the comb-drive. These capacitances are given as

$$C_{s1} = Nn \frac{\varepsilon(tl)}{d_0 + \frac{L}{L_Q} X} + C_{fringe} \quad C_{s2} = Nn \frac{\varepsilon(tl)}{d_0 - \frac{L}{L_Q} X} + C_{fringe} \quad (4.6)$$

where  $d_0$  is the initial gap between the transverse combs,  $C_{s1}$  is the decreased capacitance and  $C_{s2}$  is the increased capacitance in the transverse comb sensor corresponding to the gap change  $y = (L/L_Q)X$  and  $C_{fringe}$  is the capacitance produced due to the fringe fields. When the object

is gripped between the gripper jaws, no change in capacitance is detected by the electronic control circuitry. This indicates that the object has been grasped with avoiding any damage to the object due to excessive force applied through the actuators. The total capacitance change between differential transverse comb-drive fingers will be

$$\Delta C = C_{s2} - C_{s1} \quad (4.7)$$

The force at the tip of the jaw can be calculated in terms of the change in capacitance of the sensor by equating the total force on the electrostatic actuator fingers to the change in capacitance on the sensors fingers. During the calculation it is assumed that the central beam movement is much less than the initial gap spacing between the sensor combs fingers, i.e.  $y^2/d_0^2 \ll 1$ , the relationship is given as

$$F = \frac{Ed_0^2 t^3 \left( \frac{4b_f}{l_f^3} + \frac{b_h}{4l_h^3} + \frac{b_v}{4l_v^3} \right) \Delta C}{2Nn\epsilon(tl)} \quad (4.8)$$

where  $E$  is the modulus of elasticity of the material,  $d_0$  is the initial gap between sensor fingers,  $t$  is thickness of the device,  $\Delta C$  is change in the capacitance,  $N$  is the number of comb-drives and  $n$  is the number of capacitors. Using Eq. (4.5) and (4.8), the analytical relationship between the voltage, single jaw displacement and the force at the jaw is shown in Fig. 7. It reveals that a total of  $7.42 \mu\text{m}$  displacement and force of  $215.14 \mu\text{N}$  is obtained at the operating voltage of  $45 \text{ V}$ .

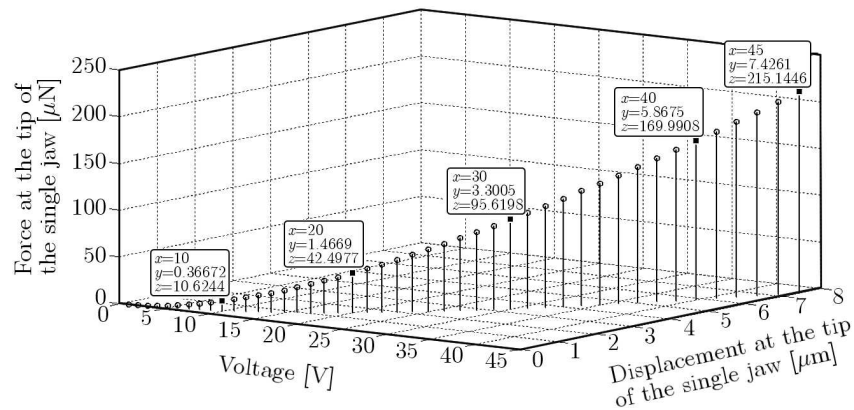


Fig. 7. Voltage vs. jaw displacement vs. force at the tip of the jaw

## 5. Design implementation and experimental results

The proposed design of the microgripper with a structural layer of  $25 \mu\text{m}$  thick single crystal silicon is fabricated using the standard MEMS process, SOIMUMPs, offered by the MEMSCAP Inc. (Miller *et al.*, 2004). Figure 8 shows the Scanning Electron Microscope (SEM) image of the fabricated microgripper. The microgripper actuator was tested at different voltages in the range of 0 to  $45 \text{ V}$  and the displacement of gripper jaws was obtained. At the actuation voltage of  $45 \text{ V}$ , a total displacement of  $16 \mu\text{m}$  was achieved at both the jaws as shown in Fig. 9. It reveals that each jaw moved by a displacement of  $8 \mu\text{m}$  that is almost the same as predicted by Eq. (4.5). Thus, the microgripper could accurately hold an object of size between  $54 \mu\text{m}$  to  $70 \mu\text{m}$  with the actuation voltage in the range of 0 to  $45 \text{ V}$  at the comb-drive based actuator.

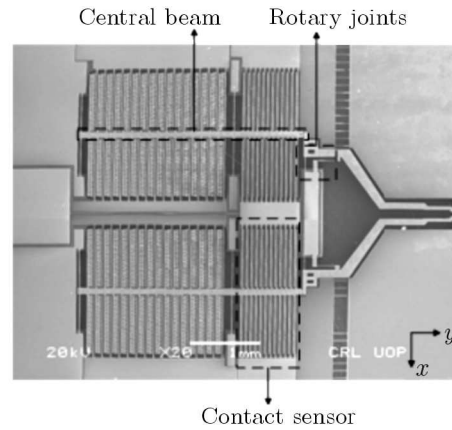


Fig. 8. SEM image of the fabricated microgripper

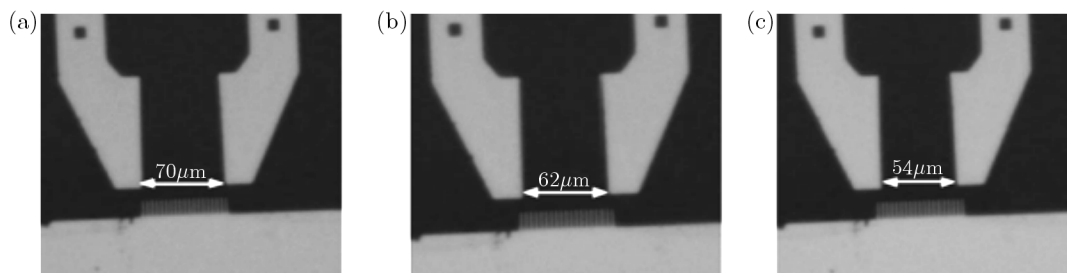


Fig. 9. Displacement at the microgripper jaws at actuation voltages of (a) 0 V, (b) 35 V, (c) 45 V

## 6. Conclusion

Design, analytical modeling, fabrication and testing of an electrostatically actuated microgripper is presented in the paper. The microgripper is fabricated using the standard SOI-MUMPs technology with a device layer of single crystal silicon having thickness of  $25\ \mu\text{m}$ . Lateral comb-drive based dual electrostatic actuation is used to produce displacement in both gripper arms simultaneously. An integrated cantilever and quad-clamped beam based compliant structure produces four times linear amplification of the displacement at the gripper jaws. The experiments demonstrate that the gripper jaws displace by  $16\ \mu\text{m}$  under the applied voltage of 45 V. The jaw design ensures full and firm grasping of micro-objects of size between  $54\ \mu\text{m}$  to  $70\ \mu\text{m}$  with the actuation voltage in the range of 0 to 45 V.

### Acknowledgment

This research work was supported by Higher Education Commission (HEC) of Pakistan under research grant No. 1012.

## References

1. BAO M., 2005, *Analysis and Design Principles of MEMS Devices*, 1st edition Elsevier
2. BEYELER F., NEILD A., OBERTI S., BELL D.J., SUN Y., DUAL J., NELSON B.J., 2007, Monolithically fabricated microgripper with integrated force sensor for manipulating microobjects and biological cells aligned in an ultrasonic field, *Journal of Microelectromechanical Systems*, **16**, 1, 7-15
3. MILLER K., COWEN A., HAMES G., HARDY B., 2004, *SOIMUMPs Design Handbook Version 4*, *Memscapinc*, available at: <http://www.memscap.com/products/mumps/soimumps/reference-material>

4. PETERSEN K.E., 1982, Silicon as a mechanical material, *Proceedings of the IEEE*, **70**, 5, 420-457
5. Universal Capacitive Readout, 2004, Universal Capacitive Readout<sup>TM</sup> IC (MS3110) Manual Irvine Sensor Corporation, available at: <http://www.irvine-sensors.com>
6. VOLLAND B.E., HEERLEIN H., RANGELOW I.W., 2002, Electrostatically driven microgripper, *Journal of Microelectronic Engineering*, **61**, 1015-1023

*Manuscript received February 26, 2013; accepted for print November 6, 2013*